JOURNAL OF MATERIALS SCIENCE 7 (1972) 72–83

Order Structures and Dislocations in Bubble Raft Grain Boundary

Y. ISHIDA*
Institute of Industrial Science, University of Tokyo, Japan

Bubble raft boundaries were examined to visualise atom configurations in the grain boundary of metals. The application of vibration to the bubble raft indicated that the boundary preferred ordered structures. Certain bubble configurations were repeated regularly along the boundary (long-range order boundary) or distributed irregularly (short-range order boundary). The orientation relationship of the former agreed with that of the coincidence-site lattice boundary, while the latter occurred only between densely packed rows of bubbles.

Various order structures occurred for each coincidence orientation. The relative stability depended on the bubble size and the vibration. Perfect and imperfect dislocations were observed in the long-range order boundary. The Burgers vector of the former is determined completely from the lattice coincidence geometry, while the vector of the latter changed with the bubble size. The boundary dislocation usually retains a step in the boundary. Therefore, glide motion of the dislocation caused grain-boundary migration by an amount equal to the step height.

1. Introduction

Experimental evidence has been accumulated that certain order structures occur in high-angle grain boundaries of metals. For an example, a regular array of boundary dislocations and fine serration were observed in the grain boundary of an annealed Fe-Mn alloy by transmission electron microscopy [14]. The same dislocation images were observed in the grain boundary of bi-crystals prepared artificially for coincidence orientation relationships [18, 24]. Earlier investigations with field ion microscopy were also able to detect micro-serrations [20] and occasional dislocations in the grain boundary [23]. These fine features can occur only when the grain boundary retains an ordered structure. They are attributed to two types of defect in the ordered grain boundary in coincidence-orientation relationship. The coincidence theory has been characterised by the elaboration on the orientational relationships of the ordered boundary [3, 4, 7, 22] and by ignoring complexities of actual atomic configurations along the boundary. The latter problem is important, since the energy of the boundary is determined actually by the atomic fit and only indirectly by the lattice fit [1].

A bubble raft is used in the present experiment to study qualitatively the atomic configurations in ordered grain boundaries and near the defect structures. The bubble raft is a simple and inexpensive model of metallic crystal structures. It has played an important role in the history of lattice-defect studies, especially of the grain-boundary structure [8-10, 19]. Other visual models have been developed (for an example, Longinov [13]), but the old model is still useful. The atomic configurations seen in the bubble raft model may now be compared with those determined by the energy calculations. The morse potential is commonly used for such calculations [12, 25]. In comparison the bubble rafter model is very qualitative, but the model accounts for some physically important factors such as many-body forces and temperature effects [10].

2. Experimental Methods

A commercial liquid soap "Raipon F" was dissolved in water in which a fine glass tube

*Now on leave at University of Surrey, England

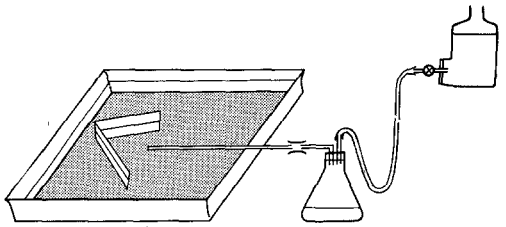

Figure 1 Apparatus for producing rafts of bubbles.

(exit diameter < 0.1 mm) was immersed to generate air bubbles of diameter $0.5 \sim 2$ mm, as shown in fig. 1. The bubble size varies with the shape and the diameter of the glass tube, the rate of the bubble generation and the depth of the glass tube tip below the water surface. A change in the bubble diameter corresponds to a change in the interatomic force distance relationship of atoms in the crystal [5]. Steady bubble generation was assured by a water reservoir about 1 m above the vessel. A commercial lapping polisher (Shinko-Syntron) was used to vibrate the vessel at 60 cycles/sec, with variable amplitude. The formation of a standing wave was avoided by placing a cloth on the rim of the vessel. To observe the glide motion of boundary-dislocations, the bubble raft boundary was sheared by tilting the vessel slightly by a finger. A 16 mm movie was used to record the glide motion. The bubble image was best when illuminated at a glancing angle to the water surface. A black surface beneath the vessel improved the bubble image.

3. Experimental Results

3.1. Formation of Order Structures

Fig. 2 is a micrograph of bubble rafts. Bubbles were generated one by one from a glass tube in the water, formed a small raft and floated away from the tube. When two small rafts met, there was usually a violent interaction involving the migration of the newly formed boundary and the emission of lattice dislocations from it. As the result, the grain boundary usually disappeared and only low-energy boundaries survived. A cyclic repetition of a bubble configuration was often noticed in such a boundary (indicated by an arrow in fig. 2). A similar ordering reaction was observed when a large bubble raft was stirred by a glass rod. A very rapid recrystallisation immediately occurred, followed by grain growth as the water was kept vibrating. Numerous small ordered regions

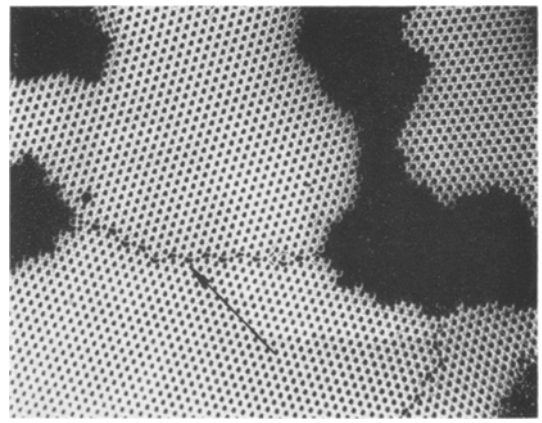

Figure 2 Occurrence of order structure in an as-grown bubble raft boundary.

appeared on the boundary. They had a tendency to grow with time.

3.2. Short and Long-range Order

Two types of order were noticed. In the grain boundary of fig. 2, the same bubble configuration is repeated regularly along the boundary. The nature of the order is of long range. In fig. 3 however, certain configurations (in circles) are scattered irregularly along the grain boundary. The nature of the order is of short range. The orientation relationship of the neighbouring grains may be described approximately by a 30° rotation about the normal to the water surface. The boundary lies between the first and the second most densely packed rows of bubbles. No similar boundary involving the third or other

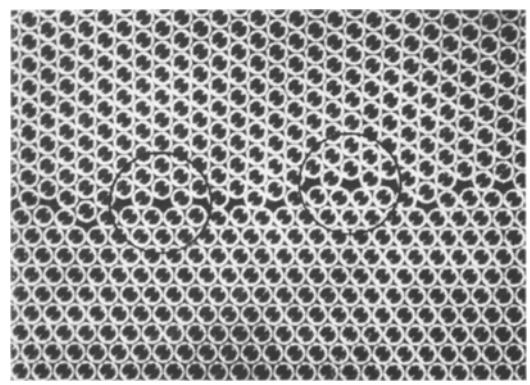

Figure 3 A bubble raft boundary with short range order. A good fit configuration occurs in an irregular manner (in circles) along the boundary. The boundary occurred between the first and the second densely packed rows of the bubble raft. Bubble diameter 1.2 mm.

less densely packed row of bubbles was observed. Grain-boundary dislocations as observed in electron micrographs cannot exist in this type of grain boundary.

The later sections are concerned only with the long range order type structures.

3.3. Bubble Configurations in the Long-range Order Boundary (coincidence boundary)

The orientation relationship of a long-range order grain boundary agrees always with that of a coincidence-site lattice boundary. However, more than one kind of bubble configuration was found for each coincidence orientation. For example, in fig. 4, all the boundaries are in $\Sigma 7$ coincidence orientation relationship: 21.8° rotation about the normal of the water surface. The Σ notation is defined by Brandon, Ralph, Ranganathan and Wald [6]. The value is the ratio between the densities of the crystal lattice sites and the coincidence sites. Although the bubble configurations are different, the spacings of the unit configurations are the same. The amount of the relative translation of the crystals, however, varies with each configuration. It is chosen so as to achieve an optimum atomic fit. The lattice-site coincidence, therefore, does not usually occur when the two crystal lattices are hypothetically extended and superimposed. The long-range order boundary is called the "coincidence boundary" only because of the characteristics of the orientational relationship.

The configurations *a* and *b* of fig. 4 are in mirror symmetry with respect to the boundary while that of *c* is not. Left and right-handed boundaries can occur with *c*. Some boundaries

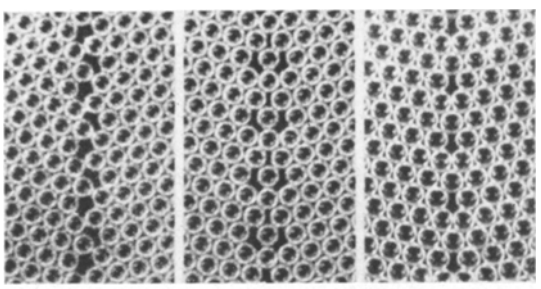

(a) (b) (c)

Figure 4 Bubble raft boundaries in $\Sigma 7$ coincidence orientation relationship. The occurrence of the configurations was determined mainly by the size of the bubble. Bubble diameter a, 1.7 mm, b and c, 0.8 mm.

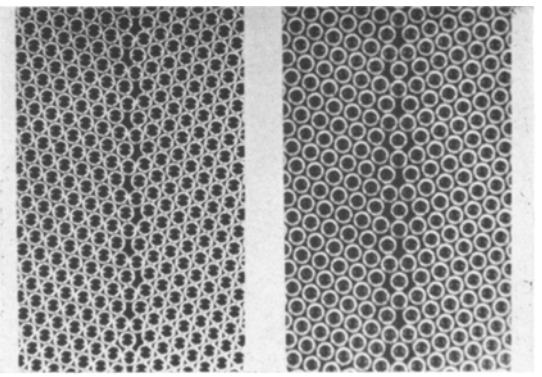

(a) (b)

Figure 5 Bubble raft boundaries in $\Sigma 13b$ coincidence orientation relationship. (a) Occurs with vibration while (b) is preferred in the absence of the vibration. (Fig. 5a is supplied by courtesy of Ookawa.)

are symmetrical but involve a translation parallel to the boundary, e.g. fig. 5b.

The occurrence of the *a* and *b* configurations of fig. 4 was determined mainly by the difference in the compressibility of the bubble as a function of bubble size [5]. Two bubbles are compressed into a site in *a*, while in *b* only one bubble stays in the corresponding site. The *a* configuration occurred when the minimum spacing between the bubbles in the raft was more than 1 mm; for smaller spacings, the *b* configuration was preferred. The two configurations can transform into each other without involving bubble diffusion if the boundary is made to migrate by imposing a small shear. The *c* configuration appears as if the two equivalent planes corresponding to {541} in fcc structure meet with little rearrangement of bubble sites; this configuration was observed when the bubble spacing in the raft was 0.8 mm. To be exact, the bubble arrangement changes slightly with the bubble size even if the type of the configuration remains the same. Two bubble configurations coexisted in certain bubble size ranges. The configuration with higher energy behaved as stacking fault to the other.

Fig. 5 is another example of order configurations, in $\Sigma 13b$ coincidence boundary. Two configurations can occur. The *a** configuration is preferred when the water was vibrated strongly while *b* was commonly observed without the vibration. The *a* configuration is more loosely bonded than the *b* configuration so that the

*Fig. 5a was selected from the photographs taken by Fukushima and Ookawa (Private communication). The other photographs were taken by the author.

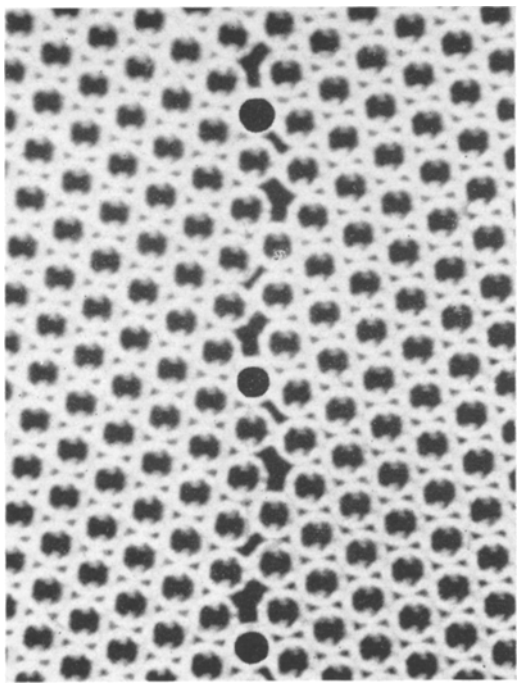

Figure 6 Bubble raft boundary in $\sum 31$ coincidence orientation relationship. Bubbles marked in black indicate the configuration unit.

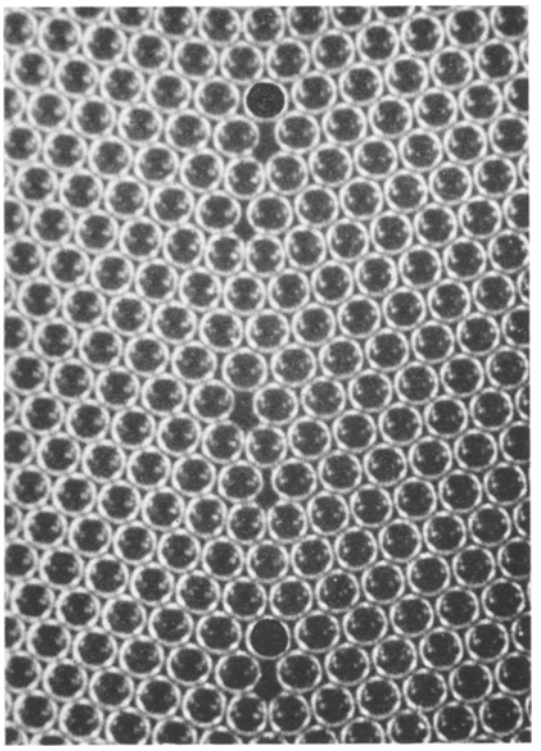

Figure 7 Bubble raft boundary in $\sum 151$ coincidence orientation relationship. The unit configuration is very large as indicated by bubbles marked in black.

bubbles in an a boundary are relatively free to vibrate.

Owing to the dimensional limitation, the bubble raft model can produce only boundaries with [1 1 1] rotation axis in the fcc structure. Among them coincidence systems with small $\sum$ values such as $\sum 7$, 13b and 19b were frequently observed. Coincidence boundaries with higher $\sum$ values were also found. For example, the boundary in fig. 6 is a $\sum 31$ coincidence boundary. A $\sum 151$ coincidence boundary is shown in fig. 7 where the unit spacing of the boundary configuration is very large, as shown marked in black.

3.4. Faceting of Coincidence Boundaries

Only certain boundary orientations are allowed with each coincidence system. The boundary, however, can assume any orientation macroscopically if it is serrated in microscopic scale by combining small areas of coincidence boundaries. Fig. 8 shows an example of atom configurations around such bending in a $\sum 7$ coincidence boundary. Boundaries in the bubble raft usually turn through 120° since three identical coincidence boundaries inclined at 60° to each other occur with coincidence systems in a [1 1 1] rotation relationship. The bubble configuration at the corner of the zigzag is complex as is shown in fig. 8. A strain-field extends into the neighbouring grains as if a dislocation lies at the corner.

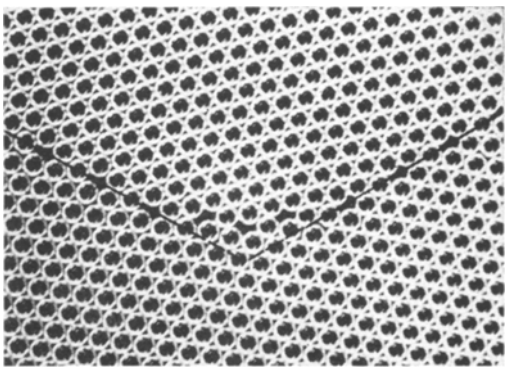

Figure 8 Disordering in the bubble configuration at the bend of a $\sum 7$ coincidence boundary. A strain field occurs round the corner when the lattice site coincidence is not achieved.

3.5 Segregation of Irregular Size Bubbles in the Coincidence Boundary

Odd-sized bubbles were often found to stay in the boundary. The segregation is caused mainly by the impeding action exerted by such bubbles against the migration of the boundary, since the diffusive motion of odd-sized bubbles is very limited. A coincidence boundary, however, is so mobile under a shear stress that the irregular-sized bubbles and even a vacancy were left in the new grain after the boundary had migrated.

3.6. Grain-boundary Dislocations

Deviations from the exact coincidence orientation relationship are accommodated by a network of boundary dislocations superimposed on the coincidence-boundary. Figs. 9 and 10 are examples of such boundary dislocations (perfect dislocations) in $\sum 7$ and $\sum 13b$ boundaries respectively. The Burgers vector of the perfect boundary dislocation is determined graphically from the coincidence plot. This method has been developed elsewhere [15]. An example is shown in fig. 11 where a $\sum 13b$ coincidence is analysed. Double circles indicate coincidence lattice sites. White and black circles are the lattice sites of the neighbouring rafts. Both lattices are extended into each other for convenience of analysis; obviously only either white or black circles are occupied on one side of the boundary once it is fixed. It has been proved geometrically that the difference vector between an arbitrary pair of

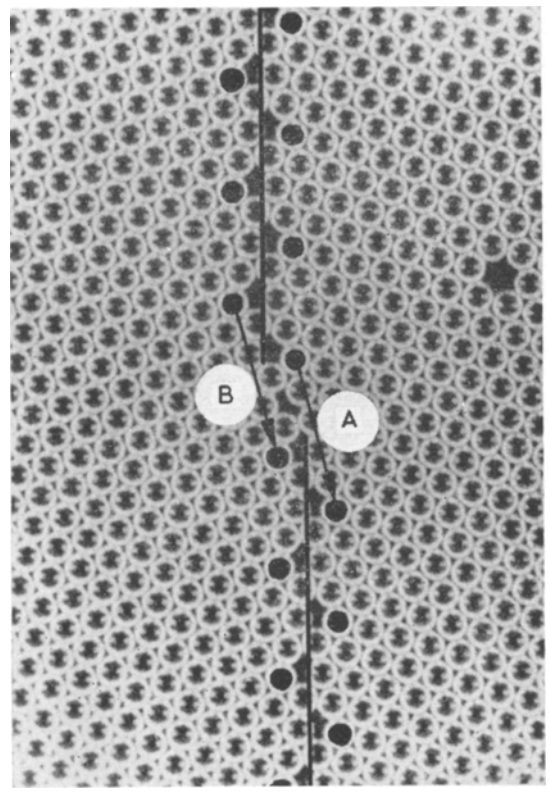

Figure 10 A boundary perfect dislocation in a $\sum 13b$ coincidence boundary. The Burgers vector $b = a/26 \langle 431 \rangle$ is equal to the difference vectors **A** and **B** in fig. 11.

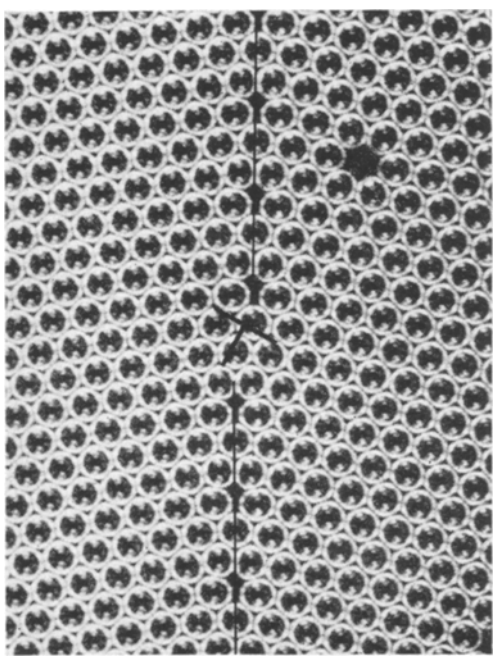

Figure 9 A boundary dislocation (a perfect edge dislocation) in a $\sum 7$ coincidence boundary. The Burgers vector $\mathbf{b} = \mathbf{a}/14 \langle 321 \rangle$ is 60° off the boundary.

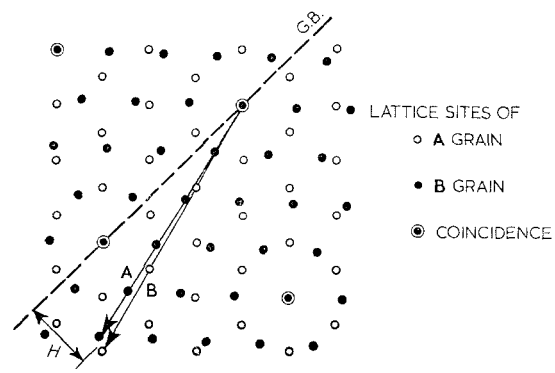

Figure 11 Coincidence plot of $\sum 13b$ bubble raft boundary. The difference vector between **A** and **B** vectors $b = a/26 \langle 431 \rangle$ equals the Burgers vector of fig. 10. The height of the dislocation step is *H*.

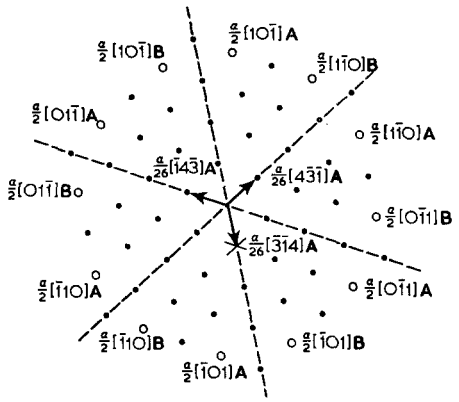

Figure 12 Burgers vectors of edge dislocations in the $\sum 13b$ coincidence bubble raft boundary. Those in white circles agree at the same time with those of lattice dislocations. Black circles are those of boundary dislocations proper.

lattice sites of the figure corresponds to the Burgers vector of a boundary dislocation [15]. Among the difference vectors those between the lattice sites of the same crystal (white circles in fig. 12) are also those of lattice dislocations while those between lattice sites of one crystal and the other (black circles) are those of boundary dislocations proper. They can exist only in the grain boundary. In fig. 12 only the Burgers vectors parallel to {1 1 1} of the fcc structure are shown. Owing to the dimensional limitation, only edge dislocations with these Burgers vectors are seen in the bubble boundary. In true metals the Burgers vector lattice is three-dimensional. The Burgers vector of the boundary dislocation in fig. 10 may be determined by comparing the identical bubble sites (marked in black as examples) on both sides of the dislocation. The difference vectors **A** and **B** may be plotted in the corresponding coincidence site as shown in fig. 11. The Burgers vector is equal to the difference between these two vectors in fig. 11. It is marked by X in fig. 12 which is 60° off the boundary line. Thus the Burgers vector of the perfect boundary dislocation is determined unambiguously from the crystal structure, the lattice spacing and the coincidence system. It is not affected by the actual bubble configuration (like those in fig. 4) or by the orientation of the boundary on which the dislocation lies. The Burgers vector of an imperfect dislocation, on the other hand, changes with the bubble size even if the type of the configurations on both sides of the imperfect dislocation does not change. Fig. 13 is an example of such an imperfect dislocation in a

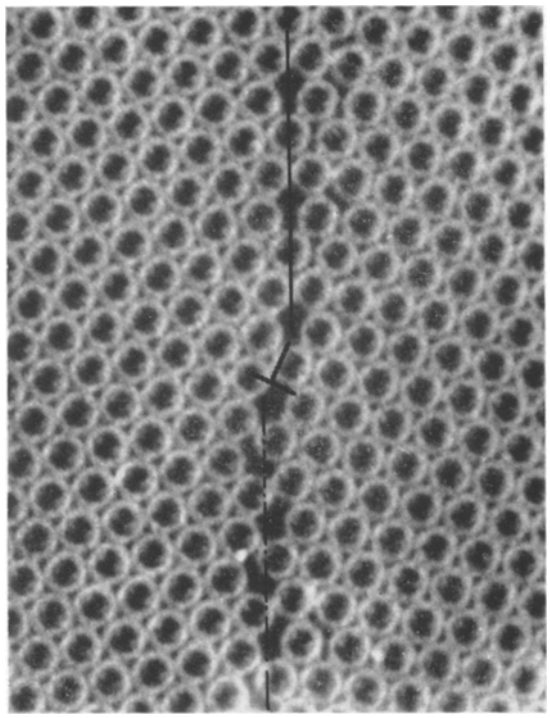

Figure 13 An example of an imperfect dislocation in a $\sum 7$ coincidence boundary. The Burgers vector changes with the bubble size.

$\sum 7$ coincidence boundary. Similarly, the strain field at the corner of the boundary serration should change with the bubble size and the type of the configuration.

Every boundary dislocation in the bubble boundary, carries a small boundary step in the core as shown in figs. 9, 10 and 13. The boundary step is inseparable from the dislocation. It is different from the micro-serration of the perfect coincidence boundary as proposed by Brandon [7] (Brandon step). The former retains a long range stress field due to the boundary dislocation while the latter does not. The height of the dislocation step is equal to the distance between the boundary and the middle point of the corresponding lattice site pair as marked H in fig. 11, while that of Brandon step is equal to the spacing of the coincidence lattice. Again, the step height of an imperfect boundary dislocation cannot be determined from the lattice geometry alone. The dislocation step would cause the boundary to deviate from the exact coincidence plane when networks of the boundary dislocation lie in it.

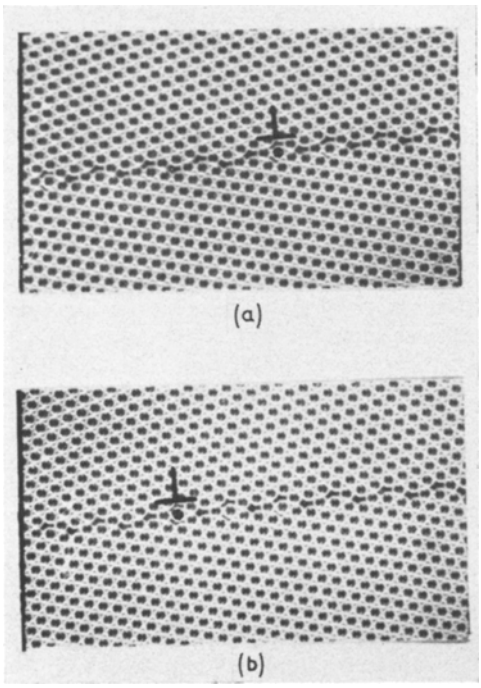

Figure 14 Slide motion of a boundary dislocation in a $\sum$13b coincidence boundary. The boundary migrated by the amount equal to the step height of the dislocation.

3.7. Glide Motion of the Boundary Dislocation

A boundary dislocation can slide only when the Burgers vector is parallel to the boundary. However, there is always at least one kind of boundary dislocation whose Burgers vector is parallel to the coincidence boundary. Fig. 14 *a* and *b* shows an example in a bubble boundary where a boundary dislocation $b=a/26\langle 431\rangle$ moved in a $\sum$13b coincidence boundary. The force required for the glide motion was larger than it would be for a lattice dislocation, but much smaller than the stress required to initiate a lattice dislocation at the edge of the bubble crystal. The large Peierls stress of the dislocation motion must be due to the complex motion of individual bubbles during the dislocation motion. The Peierls stress was lowered when the strain field of the dislocation along the boundary was wide because of boundary relaxation. When the bubble diameter was almost 1 mm, the *a* and *b* bubble configurations in fig. 4 possessed nearly equal stability so that the widening of the strain field was especially large. The boundary dislocations interacted strongly with each other. Extensive glide motion was observed only when other kinds of boundary dislocation were absent.

4. Discussion

Vibration of the bubble raft was necessary to rearrange the bubble configuration in the boundary, without this the bubble raft would correspond to metals at 0°K. The vibration, however, was not sufficient to cause vacancy diffusion. The absence of the diffusion process must have obstructed full scale realisation of order structures especially those with large $\sum$ values in the bubble raft boundary. Therefore it may be suggested that the ordering is more completely accomplished in annealed metals than in the bubble raft. It is also suggested for metals that certain impurity elements segregate regularly along the ordered boundary and lower the energy.

The short-range order boundary may agree with the island model of Mott [21]. It is interesting to know how abundant the short range order boundaries are in single phase polycrystalline specimens of metals. It appears that this type of order occurs only between densely packed planes of the metal crystal. Various high energy atomic configurations will occur around the good fit configuration so that usually the total boundary energy is not very low. However, in the interphase boundary the long range order boundary will not occur. The short-range order boundary may generally occur instead.

The bubble-size effect on the configuration in the long-range order boundary suggests the atom configurations vary with metals even if the crystal structure and the boundary orientation relationship are the same.

The amplitude of the raft vibration would correspond to the temperature. The structure with higher vibrational entropy such as the *a* configuration in fig. 5 must be more stable at higher temperatures than *b* configuration. Such structural change with temperature is likely to occur generally in the grain boundaries of metals.

A strain-field occurs at the bend of a faceted coincidence boundary, since good atomic fit and *not* lattice site coincidence is achieved at the coincidence-boundary. The component boundaries (facets) should have tendency to grow in size to reduce the overall energy of the boundary. In fact, in well annealed specimens, the facets were sometimes as large as 0.1 μm [14], while in vapour grown iron bicrystals facets as large as 10 μm were found [16]. According to FIM [20],

however, the serration is usually too fine for a transmission electron microscope to resolve. The minimum size of the serration is determined by the spacing of the coincidence lattice. The order structure and a long range stress field at the corner could not be maintained, if the size were less than several times as large as the spacing. A disordered structure equivalent to the Brandon step would occur instead.

According to the analysis of fig. 12, the magnitude of the unit Burgers vector of a boundary dislocation is smaller than that of a lattice dislocation.* The corresponding energy is small. For example, the magnitude of the Burgers vector of a boundary dislocation in fig. 10 is about $\frac{1}{4}$ of that of a lattice dislocation, so that the energy would be only of the order of $\frac{1}{16}$. The magnitude tends to decrease with increase in $\sum$ values. Therefore, boundary dislocations are likely to exist even in coincidence boundaries of large $\sum$ values. The angular range covered by a coincidence boundary together with a network of boundary dislocations, however, is small when the Burgers vector is small and the spacing of the coincidence lattice is large.

The glide motion of a boundary dislocation was limited by the faceting of the coincidence boundary. A long range sliding of the boundary dislocation is not likely to occur. The reciprocating slide motion, however, may occur and cause internal friction as proposed by Leak [17]. The reciprocating motion means a reciprocating migration of the boundary since the boundary dislocation usually retains a boundary step. The boundary dislocations move as an array so that any obstacle would suffer from a strong stress concentration from a "ready-made" pile up.

5. Conclusion

Bubble rafts are analysed to study the arrangement of atoms in the grain boundaries of single phase poly-crystals. The following conclusions are drawn;

(1) The bubble raft boundary shows preference for ordered structures. Defect structures such as boundary dislocations are defined in the ordered boundary.

(2) Long and short-range order structures were found. The orientation relationship of the former fulfilled that of the coincidence site lattice boundary. The latter occurred only between densely packed rows of bubbles in the raft.

(3) Several order configurations were found for the same coincidence orientation. Their relative stability varied with the bubble size and the presence or absence of vibration, suggesting variable atom configurations in the grain boundaries of metals even if the orientation relationship is the same.

(4) Boundary dislocations were observed. The Burgers vector of the perfect dislocation may be determined from the coincidence plot, while that of the imperfect dislocation varied with the bubble size. The dislocation usually retained a step in the boundary.

(5) Some boundary dislocations glided in shear, which resulted in migration of the boundary through a distance equal to the step height.

Acknowledgement

The author would like to thank Professor A. Ookawa for offering him a chance to examine his bubble raft micrographs and allowing him to use one of them.

References

1. K. T. AUST and B. CHALMERS, *Met. Trans.* **1** (1970) 1095.
2. W. BOLLMANN, *Phil. Mag.* **16** (1967) 363, 383.
3. *Idem*, Dislocation Dynamics (New York, McGraw-Hill, 1968) 275.
4. *Idem*, Crystal Defects and Crystalline Interfaces (Berlin, Springer, 1970).
5. W. L. BRAGG and W. M. LOMER, *Proc. Roy. Soc.* **A196** (1948) 171.
6. D. G. BRANDON, B. RALPH, S. RANGANATHAN, and W. S. WALD, *Acta Metallurgica* **12** (1964) 813.
7. D. G. BRANDON, *ibid* **14** (1966) 1479.
8. E. FUKUSHIMA and A. OOKAWA, *J. Phys. Soc. Japan* **8** (1953) 609.
9. *Idem, ibid* **9** (1954) 44.
10. *Idem, ibid* **12** (1957) 139.
11. H. GLEITER, E. HORNBOGEN, and G. BÄRO, *Acta Metallurgica* **16** (1968) 1053.
12. G. C. HASSON, J. B. GUILLOT, B. BAROUX, and C. GOUX, *Phys. Stat. Sol.* (a) **2** (1970) 551.
13. M. F. LONGINOV, *Fiz. Metall. i Metallov.* **27** (1969) 104.
14. Y. ISHIDA, T. HASEGAWA, and F. NAGATA, *J. Appl. Phys.* **40** (1969) 2182.
15. Y. ISHIDA, *Trans. Japan Inst. Met.* **11** (1970) 107.
16. *Idem* (1971), to be published.
17. G. M. LEAK, *Proc. Phys. Soc.* **78** (1961) 1520.

*Gleiter, Hornbogen and Bäro [11], on the other hand, believe the Burgers vector of a boundary dislocation (perfect dislocation) is usually larger than that of a lattice dislocation. The large Burgers vector appears energetically unreasonable, especially for coincidence boundaries of large $\sum$ values.

18. J. LEVY, *Phys. Stat. Sol.* **31** (1969) 193.
19. W. M. LOMER and J. F. NYE, *Proc. Roy. Soc.* **A212** (1952) 576.
20. R. MORGAN and B. RALPH, *Acta Metallurgica* **15** (1967) 341.
21. N. F. MOTT, *Proc. Phys. Soc.* **60** (1948) 391.
22. S. RANGANATHAN, *Acta Cryst.* **21** (1966) 197.
23. H. F. RYAN and J. SIUTER, *Acta Metallurgica* **14** (1966) 847.
24. T. SCHOBER and R. W. BALLUFFI, *Phil. Mag.* **21** (1970) 109.
25. M. WEINS, H. GLEITER, and B. CHALMERS, *Scripta Met.* **4** (1970) 235.

Received 9 July and accepted 26 July 1971.